HHS Public Access

Author manuscript

Brain Behav Immun. Author manuscript; available in PMC 2017 January 01.

Published in final edited form as:

Brain Behav Immun. 2016 January ; 51: 230–239. doi:10.1016/j.bbi.2015.08.023.

Dietary obesity reversibly induces synaptic stripping by microglia and impairs hippocampal plasticity

Shuai Hao[a], **Aditi Dey**[a], **Xiaolin Yu**[a,#], and **Alexis M. Stranahan**[a,*]

[a]Department of Neuroscience and Regenerative Medicine, Medical College of Georgia, Georgia Regents University, 1120 15th St, CA3064, Augusta, GA 30912 USA

Abstract

Obesity increases risk of age-related cognitive decline and is accompanied by peripheral inflammation. Studies in rodent models of obesity have demonstrated that impaired hippocampal function correlates with microglial activation, but the possibility that neuron/microglia interactions might be perturbed in obesity has never been directly examined. The goal of this study was to determine whether high fat diet-induced obesity promotes synaptic stripping by microglia, and whether any potential changes might be reversible by a return to low-fat diet (LFD). Time course experiments revealed that hippocampal inflammatory cytokine induction and loss of synaptic protein expression were detectable after three months of HFD, therefore subsequent groups of mice were maintained on HFD for three months before being switched to LFD for an additional two months on LFD (HFD/LFD). Additional HFD mice continued to receive HFD during this period (HFD/HFD), while another group of mice were maintained on LFD throughout the experiment (LFD/LFD). Dietary obesity impaired hippocampus-dependent memory, reduced long-term potentiation (LTP), and induced expression of the activation marker major histocompatibility complex II (MHCII) in hippocampal microglia. Diet reversal only partially attenuated increases in adiposity in HFD/LFD mice, but plasticity deficits and MHCII induction were normalized to within the range of LFD/LFD mice. Microglial activation and deficits in hippocampal function were accompanied by perturbation of spatial relationships between microglial processes and synaptic puncta. Analysis of primary microglia isolated from HFD/HFD mice revealed selective increases in internalization of synaptosomes labeled with a pH-sensitive fluorophore. Taken together, these findings indicate that dietary obesity reversibly impairs hippocampal function, and that deficits may be attributable to synaptic stripping by microglia.

Keywords

Obesity; high-fat diet; microglia; learning and memory; inflammation; phagocytosis

[*]Corresponding Author: Alexis M. Stranahan, Ph.D., Department of Neuroscience and Regenerative Medicine, Medical College of Georgia, Georgia Regents University, 1120 15th St, CA3009, Augusta, GA 30912 USA, Ph: (706) 721-7885, Fax: (706) 434-7823, astranahan@gru.edu.

[#]Current address: Shandong University, No. 44 Wenhuaxi Road, Jinan, Shandong, China, 250012

1. Introduction

Obesity is associated with chronic systemic inflammation and has also been shown to increase risk of age-related cognitive decline (Kanneganti and Dixit, 2012; Whitmer et al., 2008; Xu et al., 2011). While the pathogenesis of metabolic comorbidities in obesity is well-characterized, cellular mechanisms for cognitive impairment in obesity remain less so. Multiple reports indicate that that high-fat diet (HFD)-induced obesity impairs cognitive function in rodent models (Molteni et al., 2002; Stranahan et al., 2008; McNay et al., 2010). Because hippocampal neurons exhibit early vulnerability during age-related cognitive impairment, studies of cognitive dysfunction in obesity have primarily focused on differences in hippocampal synaptic plasticity. Parallel observations by multiple groups now support the idea that obesity-induced systemic inflammation is accompanied by inflammation in multiple brain regions, including the hippocampus (Erion et al., 2014; Buckman et al., 2014; Sobesky et al., 2014).

Microglia are brain-resident phagocytes that continuously monitor the neuropil with motile processes for detection and clearance of cellular debris. In addition to removing dead cells and extracellular aggregates, microglia also internalize synaptic terminals (Kettenman et al., 2013). Synaptic internalization by microglia is critical for developmental synaptic pruning (Paolicelli et al., 2011) and evidence from the visual cortex indicates that this process is activity-dependent (Tremblay et al., 2010). Microglia/neuron interactions are not limited to internalization or ‘stripping,’ as a number of signaling pathways that attract microglia to inactive synapses have now been identified (Stevens et al., 2007; Schafer et al., 2012). Microglia also influence plasticity through local release of neurotrophins at dendritic spines (Parkhurst et al., 2013), but the idea that synapse loss in obesity might be mediated by microglia has never been directly examined.

These studies were designed to determine whether interactions between microglia and neurons might be altered in dietary obesity. To answer this question, we used mice exposed to high-fat diet (HFD/HFD), low-fat diet (LFD/LFD), or HFD followed by LFD (HFD/LFD). The duration of HFD applied prior to diet reversal was determined in time course experiments, which identified 3 months of HFD as the onset of inflammatory cytokine accumulation and loss of hippocampal synaptic proteins. Concurrent measures of adiposity and insulin resistance revealed that hippocampal inflammation and synaptic loss occurred after the development of obesity, but before the onset of diabetes. The diet reversal experiments revealed that a return to LFD normalizes hippocampus-dependent memory, long-term potentiation (LTP), and spatial relationships between microglia and hippocampal synapses. Experiments in primary microglia from LFD/LFD, HFD/HFD, and HFD/LFD mice identified selective, obesity-induced increases in microglial internalization of synaptosomes labeled with a pH-sensitive fluorophore. Taken together, these results indicate that obesity reversibly increases synaptic internalization by microglia, and implicate this process as a mechanism for impaired hippocampal function.

2. Materials and Methods

2.1. Animals and diets

Male C57Bl6J mice were purchased from Jackson Laboratories (Bar Harbor, Maine) at 5 weeks of age. After one week acclimation, mice were housed one per cage, with high-fat diet chow (HFD; Research Diets 12492) or low-fat diet chow (LFD; Research Diets 12450J) and water available ad libitum (see Supplementary Table 1 for diet composition). For the time course experiments, (n=6–7) mice were maintained on HFD or LFD for one, two, or three months, with food intake measured on two successive days per week and body weights collected weekly. One week before euthanasia, mice were fasted overnight for analysis of glucose and insulin levels, as described (Dey et al., 2014). At sacrifice, the weights of the epididymal fat pads were collected as a measure of visceral adipose tissue and the inguinal depot was weighed as a measure of subcutaneous fat. Hippocampal protein extracts from mice exposed to different durations of HFD or LFD were collected to measure interleukin 1β (IL1β) protein and synaptic marker expression.

For diet reversal experiments, mice were maintained on HFD for three months before being switched to LFD chow for two months (HFD/LFD) or continued availability of HFD chow (HFD/HFD). Additional groups consumed LFD chow throughout all five months of the experiment (LFD/LFD). For immunofluorescence and stereology, (n=8) mice from each condition were transcardially perfused with 4% paraformaldehyde in phosphate buffer (PFA). For analysis of long-term potentiation and dendritic spine density, (n=8–11) from each condition were rapidly decapitated under light Isoflurane anesthesia for preparation of acute slices (described below). Additional groups of (n=12) mice per condition were transcardially perfused with sterile saline for isolation of primary microglia by density gradient centrifugation, as described (Erion et al., 2014; Dey et al., 2014). All cohorts of mice generated for these experiments were used for behavioral tests of hippocampus-dependent memory.

2.2. Behavioral testing

Groups of mice from each cohort were tested in the Y-maze and novel object preference tests. Testing in both paradigms was carried out between 1800 and 2200hr (lights-off at 1800) under red light illumination, as described (Erion et al., 2014; Wosiski-Kuhn et al., 2014). For Y-maze testing, mice were transferred from the home cage into a randomly selected start arm (length × width × height, cm: 20 × 6 × 10). Each alternation trial consisted of free exploration until a complete arm entry. After entering the choice arm, mice were confined to that arm by lowering a guillotine door during a 1-minute inter-trial interval before beginning the next trial. Each of the (6) alternation trials was captured on digital video and video clips were coded for offline analysis in a blinded manner. Correct choices were expressed relative to the total number of potential alternations and used for subsequent statistical analysis.

Novel object recognition testing involved 10min exposure to two identical objects, followed by 30min in the home cage, after which the mouse was returned to the arena in the presence of one novel and one familiar object. After 5min object exploration, the mouse returned to

the home cage for 1.5hr before re-exposure to the familiar object and a different novel object. Test sessions were captured on video and analyzed offline at half speed by an observer blinded to the treatment conditions. The duration of each exploratory interval was recorded and expressed relative to the total amount of object exploration (novel + familiar) for each trial.

2.3. Hippocampal slice preparation and electrophysiology

Hippocampal slice preparation and extracellular recording followed previously published methods (Wosiski-Kuhn and Stranahan, 2012). In brief, 300μm slices were cut on a Vibratome (Leica, Buffalo Grove, IL, USA) into a bath of oxygenated artificial cerebrospinal fluid (ACSF). After 1hr recovery at 37C, extracellular recordings were performed in ACSF supplemented with 50μM picrotoxin (Sigma-Aldrich, St. Louis, MO, USA). Electrodes were positioned in the middle molecular layer superficial to the dentate gyrus and medial perforant path inputs were functionally identified by the presence of paired-pulse depression (PPD; Asztely et al., 2000). PPD magnitude was determined using interpulse intervals of 50, 200, 500, and 1000msec, and quantified by expressing the slope of the second (S2) field excitatory postsynaptic potential (fEPSP) as a percent of the first fEPSP (S1). The baseline stimulation intensity was set at 50% of maximal fEPSP slope generated from the input/output curve. Stimuli were delivered at 0.05 Hz for baseline and post-tetanus recording and LTP was induced with a single train delivered at 100 Hz for 1 second. Data were collected using pClamp version 10.3.4 and analyzed in Clampfit (Molecular Devices, Sunnyvale, CA, USA).

2.4. DiI labeling, dendrite imaging, and quantification of dendritic spine density

Juxtacellular labeling with the lipophilic membrane tracer 1,1′-dioctadecyl-3,3,3′,3′-tetramethyl-indocarbocyanine perchlorate (DiI; Invitrogen, Carlsbad, CA) followed previously published methods (Wosiski-Kuhn et al., 2014). In brief, hippocampal slices were generated as described above, but instead of recording, slices were fixed in PFA for 1hr and DiI crystals were placed in the dentate hilus inferior to the dentate granule cell layer. Following 48hr incubation at 37C, slices were counterstained with DAPI (1:1,000, Sigma-Aldrich) and z-stack images of dendritic segments were acquired through an oil immersion objective (NA 1.4) on a Zeiss LSM510 Meta confocal microscope.

Dendritic segments were sampled from the secondary and tertiary dendrites of dentate gyrus granule neurons, as described (Erion et al., 2014; Wosiski-Kuhn et al., 2014). Full-resolution images of each plane were imported into Reconstruct (http://synapses.clm.utexas.edu) for spine counting and three-dimensional length measurement of each sampled segment. Segments were averaged on a per-cell basis, and the mean spine density across 5–7 cells from each animal was used for statistical analysis.

2.5. Immunohistochemistry and unbiased stereology

Peroxidase immunohistochemistry for ionized calcium binding adaptor protein 1 (IBA1) was carried out according to previously published methods (Dey et al., 2014). Briefly, a 1:6 series of 40 μm sections was collected using a freezing microtome (Leica) and stored in cryoprotectant at −20C. Free-floating tissue sections were washed in phosphate buffered

saline (PBS), quenched in 0.3%H2O2, blocked in 5% goat serum, and incubated overnight in PBS containing 0.25% Tween-20 and rabbit anti-IBA1 (Wako Diagnostics). The next day, sections were rinsed, then incubated with biotinylated anti-rabbit, and rinsed again before avidin-biotin amplification and detection with diaminobenzadine (Vector Labs, Burlingame, CA). Slides were dried and counterstained with Methyl Green (Sigma-Aldrich, St. Louis, MO, USA) before dehydration, clearing, and coverslipping under Permount. Stereological cell counts based on the optical fractionator were carried out using StereoInvestigator software (Microbrightfield, VT, USA). IBA1-positive cells in the dentate gyrus were counted using systematic random sampling, with an XY step size of 300 μm and a counting frame measuring 50 μm on each side (height =10 μm). Separate markers were used for microglia with 1 or 2 primary processes ('Simple') or microglia with 3 or more processes ('Complex'). Anatomical criteria for Simple and Complex microglia were based on internal validation of previous reports demonstrating that hippocampal microglia in sections from unstimulated mice have an average of 3.9±0.8 primary processes (Giovanoli et al., 2013). The results reported by Giovanoli et al (2013) were internally validated by manually reconstructing IBA1+ cells in the dentate molecular layer of LFD mice used in the current study, which revealed similar results (n primary processes; mean±sem: 4.3±0.9). All counts were performed blind on coded slides and the code was not broken until completion of the stereology experiments.

2.6. Immunofluorescence and confocal microscopy

Double-labeling immunofluorescence for IBA1 and major histocompatibility complex II (MHCII), a marker of classical activation, took place as described (Erion et al., 2014). In brief, free-floating sections were quenched in 1% sodium borohydride in tris-buffered saline (TBS), blocked in normal sera, and incubated with primary antibodies against IBA1 (1:1,000, Wako) and MHCII (1:500, Abd Serotec) diluted in TBS with 0.1% Triton-X 100. The following day, sections were washed in TBS, then reacted with fluorophore-conjugated secondary antibodies (Invitrogen, Carlsbad, CA) before being mounted on slides. After drying, slides were counterstained with DAPI and coverslipped for confocal imaging using a 63x objective on a Zeiss LSM510 Meta confocal microscope. Image stacks containing IBA1-positive microglia with 1 or 2 primary processes ('Simple') or microglia with 3 or more processes ('Complex') were acquired throughout the rostrocaudal extent of the dentate molecular layer. The proportion of IBA1/MHCII double-positive cells ('Simple' or 'Complex') was expressed relative to the total number of simple or complex IBA1-positive cells. Immunohistochemical controls included omission of primary and secondary antibodies and routinely revealed no detectable fluorescence in tissue sections.

Immunofluorescence was also used to detect IBA1 and postsynaptic density 95 (PSD95) for analysis of spatial relationships between microglial processes and synaptic puncta. The immunofluorescence procedure used the same polyclonal antibody to IBA1 (1:1,000, Wako) and a monoclonal antibody against PSD95 (1:500, Pierce Thermo Fisher). Bound primary antibodies were visualized using fluorescent secondary antibodies (Invitrogen), and nuclei were counterstained with DAPI. Image stacks were captured from the dentate molecular layer at 1024×1024 pixel density (0.1μm step size) using a 100x oil immersion objective

(NA 1.4). The pinhole diameter was reduced to 420.42nm to maximize resolution and IBA1+ processes were sampled at least 25μm from the cell body.

Multichannel Sholl analysis was used to examine spatial relationships between PSD95+ puncta and IBA1+ microglial processes. Three-dimensional centroid coordinates for IBA1+ processes were determined automatically using an ImageJ plugin, as described (Bolte et al., 2006), and numbers of PSD95+ puncta were quantified at progressively increasing spherical diameters around the centroid coordinates. To generate a measure of proximity that would not reflect overall reductions in PSD95 labeling, the number of PSD95+ intersections for each sphere was normalized to the number of intersections at the smallest spherical shell diameter. The normalized number of PSD95+ intersections at progressively increasing distances around IBA1+ processes were generated from >400 processes sampled from 12–16 fields in each mouse, and the slope of this relationship was averaged on a per-animal basis for statistical comparisons.

2.7. Western blotting and ELISA

Protein extraction and quantification of total protein by Bradford assay took place as described (Wosiski-Kuhn et al., 2014). In brief, hippocampal protein extracts (20μg) were loaded and separated through gel electrophoresis. Proteins were transferred to nitrocellulose membranes, blocked in 5% nonfat milk, and probed with antibodies against spinophilin (Millipore, Temecula, CA, USA), PSD95 (Pierce Thermo Fisher), synaptophysin (Sigma-Aldrich, St. Louis, MO, USA), TATA-binding protein (TBP; Cell Signaling Technologies, Danvers, MA, USA), or β-actin (Sigma-Aldrich, St. Louis, MO, USA). Primary antibodies were applied at 1:1,000 overnight with shaking at 4C and detected with HRP-conjugated secondaries against the appropriate species. Bands were visualized on a chemiluminescence imager and band intensities were quantified in ImageJ. Enzyme-linked immunosorbent assay was used to quantify interleukin 1β in hippocampal protein extracts according to the manufacturer's instructions (R&D Systems, Minneapolis, MN) and as described (Dey et al., 2014; Erion et al., 2014).

2.8. Synaptosome preparation and pHrodo incorporation

Purified synaptosomes were separated by ultracentrifugation on a discontinuous isoosmotic Percoll gradient. Methods for synaptosome isolation were based on previously published protocols (Dunkley et al., 2008; Meffert et al., 1994). Mice were terminally anesthetized with Isoflurane and transcardially perfused with 25mL sterile saline for 3min before forebrain extraction and homogenization of individual hemispheres in a Tenbroeck homogenizer containing 5mL Dulbecco's phosphate-buffered saline (dPBS) supplemented with 0.2% d-glucose. Homogenized cell suspensions were filtered through a 40-micron strainer (BD Bioscience) and the flow-through was centrifuged at 1,000xg for 10min to pellet cells. The pellet (P1) was either lysed for westerns or fixed for electron microscopy, and the supernatant (S1) was layered on top of the Percoll gradient in preparation for ultracentrifugation. For some experiments, aliquots of supernatant were lysed for western blotting or fixed for electron microscopy; for others, a portion of the S1 was reserved for incorporation of the pH-sensitive fluorophore pHrodo Green (Molecular Probes, Carlsbad, CA, USA).

Density gradients were separated at 28,000xg for 5min at 4C with no brake on a Beckman-Coulter ultracentrifuge equipped with a fixed-angle TY65 rotor. The 23%/10% interface containing purified synaptosomes was collected and transferred to a fresh tube containing dPBS with 0.2% d-glucose. After inversion, resuspended synaptosomes were pelleted by ultracentrifugation at 28,000xg for 10min with full brake and used for western blotting, electron microscopy, or pHrodo incorporation (see below).

The relative enrichment of synaptic and nuclear markers was determined by western blotting of purified synaptosomes and S1 or P1 fractions. Protein separation, transfer, and quantification of each fraction followed the same methods described above for brain tissue lysates. Fractions used for electron microscopy were resuspended in 2.5% glutaraldehyde in 0.1M cacodylate buffer containing 2mM Ca2+. After fixation, fractions were pelleted and washed with cacodylate buffer before dehydration and en bloc staining with 2% uranyl acetate. After further dehydration in 70, 95, and 100% ethanol, samples were embedded in Epon-Araldite resin and cured for 2 days at 60C in preparation for ultrathin sectioning (75nm). Ultrathin sections were cut with a diamond knife on a Leica EM UC6 ultramicrotome (Leica Microsystems, Inc, Bannockburn, IL), collected on copper grids and stained with uranyl acetate and lead citrate before imaging on a JEM 1230 transmission electron microscope (JEOL USA Inc., Peabody, MA), as described (Wosiski-Kuhn et al., 2014).

For fluorophore incorporation, purified synaptosomes or S1 fractions were incubated with pHrodo Green STP ester, as described (Schafer et al., 2012), with modifications. Specifically, aliquots from each fraction were rapidly lysed and used to determine protein content by Bradford assay. Appropriate volumes of S1 and purified synaptosomes were resuspended at 20mg/mL in 100mM carbonate buffer (pH=9.0). pHrodo Green in DMSO was added at a final concentration of 8.9mM and fractions were incubated for 1hr at room temperature with gentle agitation. Samples were washed through 3 rounds of centrifugation (5min, 15,000xg, 4C) in carbonate buffer, with the final resuspension made in dPBS containing 5%DMSO. Fractions were stored in dPBS+DMSO at −80C in preparation for experiments in primary microglia.

2.9. Primary microglia isolation and analysis of phagocytosis

Primary microglia were isolated from HFD/HFD, HFD/LFD, and LFD/LFD mice according to previously published protocols (Erion et al., 2014; Dey et al., 2014). In brief, animals were transcardially perfused with saline as described above for synaptosome preparation, with preparation of cell suspensions using identical methodology. After the initial round of centrifugation, forebrain mononuclear cells were separated by centrifugation on a discontinuous gradient of isoosmotic Percoll. The 70%/30% interface was collected and washed in 1xdPBS before determination of yield and viability using a Scepter automated counting instrument (Millipore), as described (Dey et al., 2014).

Peritoneal macrophages were isolated from a subset of animals used for preparation of primary microglia. The isolation procedure did not require thioglycollate stimulation and involved peritoneal lavage with dPBS containing 5% heat-inactivated fetal bovine serum (Gibco, Carlsbad, CA). Cells collected by lavage were pelleted by 10min centrifugation at

1,000xg and counted using methods described above for microglia. Both cell types were plated at 100,000 cells/well in serum-free DMEM for phagocytosis assays. pHrodo-conjugated e.coli particles were applied at 1mg/mL in 1X dPBS (pH=7.4). pHrodo-conjugated synaptosomes and S1 fractions were thawed to 37C in dPBS+DMSO and applied at 20mg/mL. Cells were exposed to pHrodo-conjugated stimuli for 2hr at 37C under 5% CO2 before being washed in dPBS and read in a fluorescent plate reader (Biotek Instruments, VT, USA). Fluorescence intensities were normalized to the average intensity detected in control wells from each animal. Control wells were run in duplicate and contained either pHrodo-conjugated stimuli with no plated cells, or plated cells not exposed to pHrodo-conjugated stimuli.

In a subset of these experiments, primary microglia were plated on 35mm dishes with embedded coverslips for visualization of internalized pHrodo-conjugated e.coli particles (Invitrogen, Temecula, CA, USA). For this subset, cells were fixed for 30min in 2% paraformaldehyde before staining with rabbit anti-IBA1 (Wako) and Alexa 568 anti-rabbit (Invitrogen), followed by counterstaining with DAPI for multiphoton imaging on a Zeiss 780 inverted confocal microscope.

2.10. Statistics

Body weights and food intake data were compared across conditions using one-way repeated measures ANOVA. Dendritic spine densities and western blot endpoints were analyzed using one-way ANOVA, as were the electrophysiological data and data from the phagocytosis assays. Stereological counts of hippocampal microglia and colabeling with activation markers were also analyzed with one-way ANOVA. For analysis of spatial relationships between microglial processes and synaptic puncta, per-animal slopes for the normalized number of PSD95+ intersections at progressively increasing distances around IBA1+ processes were generated using nonlinear regression, and slopes were compared across conditions using one-way ANOVA as described above. Analysis by ANOVA was followed by post hoc comparisons with Bonferroni-corrected t-tests, with $p<0.05$ as the threshold for statistical significance. Analyses were carried out in Graphpad Prism version 5.0 (La Jolla, CA).

3. Results

3.1. Time course for obesity, neuroinflammation, and hippocampal synaptic deficits

We initially performed time course experiments to determine the onset of hippocampal inflammation and synaptic loss relative to obesity and diabetes. Male C57Bl6J mice were maintained on high-fat diet (HFD) chow or low-fat diet (LFD) chow for one, two, or three months, beginning at six weeks of age (see Supplementary Table 1 for diet composition). Increases in body weight were detected in HFD mice at all time points examined ($F_{1,18}=10.85$, $p<0.01$; Supplementary Figure 1A). At sacrifice, the visceral and subcutaneous fat pads were dissected to examine adipose tissue distribution. The relative weight of the visceral fat pads increased in a time-dependent manner ($F_{1,18}=8.11$, $p<0.01$; Supplementary Figure 1B), while the subcutaneous fat pads exhibited similar hypertrophy at all time points ($F_{1,18}=7.13$, $p<0.01$, Supplementary Figure 1C). HFD mice reduced the

amount of food eaten and were isocaloric with LFD mice throughout the experiment ($F_{1,18}$=0.24, ns; Supplementary Figure 1D), and there were no significant changes in fasting glucose ($F_{1,18}$=1.52, ns; Supplementary Figure 1E) or insulin ($F_{1,18}$=1.91, ns, Supplementary Figure 1F). These observations indicate that these durations of HFD consumption elicit obesity prior to the onset of diabetes symptoms.

We next quantified interleukin 1β (IL1β) protein in hippocampal homogenates from mice exposed to different durations of HFD. Three months of HFD significantly increased hippocampal IL1β ($F_{1,18}$=7.98, $p<0.05$; Supplementary Figure 2A), with no effect of HFD at earlier time points. These samples were also used to examine hippocampal synaptic protein expression. Western blotting for the postsynaptic marker PSD95 and the presynaptic marker synaptophysin revealed that expression of both markers was reduced after 3 months on HFD (for PSD95, $F_{1,18}$=3.84, $p<0.05$; for synaptophysin, $F_{1,18}$=5.13, $p<0.05$; Supplementary Figure 2B–D). Because three months of HFD increased hippocampal IL1β and reduced expression of synaptic proteins, this duration of HFD was selected for subsequent diet reversal experiments.

3.2. Body weight and adiposity after a switch from high-fat to low-fat feeding

We next examined the effects of switching mice from HFD to LFD on body weight, food intake, and adiposity. Six-week-old mice were maintained on LFD or HFD for three months, then half of the HFD mice were switched to LFD chow for an additional two months before sacrifice (HFD/LFD). The switch to LFD chow was associated with gradual reductions in body weight in HFD/LFD mice ($F_{2,21}$=9.88, $p<0.01$; Figure 1A), which occurred independently of changes in overall caloric intake ($F_{2,21}$=0.24, ns; Figure 1B). Examination of adipose tissue distribution revealed that diet reversal reduces visceral and subcutaneous adiposity relative to mice that continued to consume HFD throughout the experiment (for visceral fat, $F_{2,21}$=8.62, $p<0.01$; for subcutaneous fat, $F_{2,21}$=6.99, $p<0.05$). However, the proportional weight of both visceral and subcutaneous fat after the switch is still significantly greater than LFD/LFD mice (post hoc t-tests with Bonferroni's correction: visceral fat, t_{13}=12.68, $p<0.01$; subcutaneous fat t_{13}=7.94, $p<0.01$; Figure 1C). In these respects, the return to LFD feeding attenuates but does not reverse the physiological consequences of long-term HFD consumption.

3.3. High-fat diet consumption reversibly activates hippocampal microglia

Microglia respond to inflammation by retracting their processes and expressing classical activation markers (Prinz and Priller, 2014). We used unbiased stereology to examine changes in microglial number and morphology in the hippocampal dentate gyrus of HFD/HFD, HFD/LFD, or LFD/LFD mice. Microglia were visualized using antibodies against IBA1 and anatomically 'simple' microglia with 1–2 primary processes were quantified separately from 'complex' microglia bearing ≥3 primary processes. HFD/HFD mice had significantly more anatomically simple IBA1+ cells in the dentate molecular layer and granule cell layer, relative to both LFD/LFD and HFD/LFD mice ($F_{2,18}$=4.47, $p<0.05$; Figure 2A–B). There were no changes in the number of complex microglia ($F_{2,18}$=0.62, ns), and while there was a trend towards increased total IBA1+ cell number in HFD mice, this

did not reach statistical significance (mean±sem, n=6–8; LFD/LFD=19,152±2,416; HFD/HFD=24,013±2,598; HFD/LFD=21,328±3,409).

We examined cellular activation in simple and complex microglia using co-labeling for IBA1 and major histocompatibility complex II (MHCII). Positive staining for MHCII was minimal on hippocampal sections from LFD/LFD mice, but simple microglia from HFD/HFD mice showed significant increases in MHCII expression ($F_{2,18}$=8.57, p<0.01; Figure 2C). MHCII induction was not observed in HFD/LFD mice (Figure 2D), indicating that obesity reversibly activates anatomically simple microglia in the hippocampal dentate gyrus.

3.4. Diet reversal normalizes synaptic plasticity and cognition

To determine whether reductions in microglial activation with diet reversal were accompanied by reinstatement of hippocampal plasticity, we recorded long-term potentiation (LTP) in hippocampal slices from LFD/LFD, HFD/HFD, or HFD/LFD mice. Recordings were made at medial perforant path (mPP) inputs to the hippocampal dentate gyrus, which were identified anatomically by their location in the middle molecular layer, and functionally by the presence of presynaptic paired-pulse depression (PPD; Asztely et al., 2000). Analysis of the input-output ratio revealed no differences between experimental groups ($F_{2,22}$=0.24, ns; Figure 3A), and PPD magnitude was unchanged ($F_{2,22}$=0.68, ns; Figure 3B). However, slices from HFD/HFD mice exhibit reduced LTP relative to slices from LFD/LFD mice ($F_{2,22}$=8.51, p<0.01; Figure 3C). LTP deficits were not detected in HFD/LFD mice, which were indistinguishable from LFD/LFD slices (post hoc t-tests with Bonferroni's correction: t_{15}=0.48, ns; Figure 3C). These results indicate that dietary obesity reversibly impairs hippocampal synaptic plasticity, and implicate postsynaptic changes as a mechanism for HFD-induced deficits.

To examine the behavioral consequences of impaired synaptic plasticity, we analyzed hippocampus-dependent memory in LFD/LFD, HFD/HFD, and HFD/LFD mice. Spatial recognition memory was significantly impaired in HFD/HFD mice, based on reduced alternation during testing in the Y-maze ($F_{2,24}$=9.81, p<0.01; Figure 3D). Deficits in spatial memory were not observed in HFD/LFD mice, which performed similarly to LFD/LFD mice (post hoc t-tests with Bonferroni's correction: t_{15}=1.14, ns; Figure 3D). Mice were also tested in the novel object recognition paradigm, where HFD/HFD mice showed less preference for the novel object at all post-training intervals ($F_{2,24}$=6.23, p<0.05; Figure 3E). Diet reversal normalized object recognition, based on comparable preference for the novel object in HFD/LFD and LFD/LFD mice (post hoc t-tests with Bonferroni's correction: t_{15}=0.37, ns; Figure 3E). All experimental groups spent similar total time exploring the objects (novel+familiar), indicating that changes in novel object preference are not explained by differences in motivation (Figure 3F). Taken together, these behavioral results suggest that dietary obesity induces memory deficits that are reversible following a return to LFD.

3.5. Dietary obesity perturbs spatial relationships between microglia and synapses

We next examined hippocampal structural plasticity by quantifying dendritic spine density using juxtacellular labeling with the lipophilic membrane tracer DiI. This experiment revealed significant reductions in dendritic spine density in HFD/HFD mice, relative to LFD/LFD mice ($F_{2,21}$=9.76, p<0.01; Figure 4A–B). There were no differences in dendritic spine density between LFD/LFD and HFD/LFD mice (post hoc t-tests with Bonferroni's correction: t_{16}=0.55, ns; Figure 4B), indicating that reinstatement of synaptic function was accompanied by reversal of synaptic loss. Western blotting for pre- and postsynaptic proteins revealed that HFD/HFD significantly reduced expression of the presynaptic protein synaptophysin ($F_{2,19}$=6.56, p<0.05), the postsynaptic protein PSD95 ($F_{2,19}$=5.24, p<0.05) and the scaffolding protein spinophilin in hippocampal homogenates ($F_{2,19}$=7.31, p<0.05; Figure 4C–D). Reductions in synaptic protein expression were not present in HFD/LFD mice (post hoc t-tests with Bonferroni's correction: for synaptophysin, t_{11}=0.36, ns; for PSD95, t_{11}=0.85, ns; for spinophilin, t_{11}=0.53, ns; Figure 4D). These results provide anatomical and cellular evidence for hippocampal synaptic loss in obesity.

To examine spatial relationships between microglial processes and hippocampal synapses, PSD95-labeled puncta and IBA1-positive processes were visualized in the dentate molecular layer. Multichannel Sholl analysis was used to examine spatial proximity of PSD95+ puncta around IBA1+ microglial processes. Three-dimensional centroid coordinates for IBA1+ processes were determined automatically using an ImageJ plugin, as described (Bolte et al., 2006), and numbers of PSD95+ puncta were quantified at progressively increasing spherical diameters around the centroid coordinates.

Single-channel analysis of PSD95 labeling revealed that HFD/HFD reduces the area covered by PSD95+ puncta ($F_{2,19}$=7.10, p<0.05; Figure 4E–F). To generate a measure of proximity that would not reflect overall reductions in PSD95 labeling in HFD/HFD mice, the number of PSD95+ intersections for each sphere was normalized to the smallest spherical shell diameter. This approach revealed that synaptic density is significantly higher in the immediate vicinity of microglial processes in LFD/LFD mice, based on decreasing numbers of intersections with PSD95 puncta at greater spatial distances from IBA1 centroid coordinates (Figure 4G; nonlinear fit of normalized intersections around IBA1 centroid in LFD/LFD mice: r^2=0.79, p<0.01). Interestingly, the positive correlation between IBA1 process proximity and PSD95 puncta is lost in HFD/HFD mice (nonlinear fit of normalized intersections around IBA1 centroid in HFD/HFD mice: r^2=0.13, ns). HFD/LFD mice, by contrast, exhibit the same spatial relationship between synaptic puncta and microglial processes observed in LFD/LFD mice (nonlinear fit of normalized intersections around IBA1 centroid in HFD/LFD mice: r^2=0.73, p<0.01). This anatomical pattern suggests that the spatial organization of microglial processes around hippocampal synapses may be disturbed in dietary obesity, and this was upheld by statistical comparison of group differences ($F_{2,19}$=4.53, p<0.05).

3.6. Dietary obesity promotes synaptic stripping by microglia

Microglia internalize synapses during activity-dependent plasticity in the developing brain (Tremblay et al., 2010), but synaptic phagocytosis by microglia has never been examined in

any model of obesity. We prepared synaptosomes for in vitro analysis of synaptic stripping and initially validated the purity of this preparation using western blotting and electron microscopy. Isolated synaptosomes were enriched with PSD95 and synaptophysin (Figure 5A). These synaptic proteins were diluted in the S1 fraction and were absent in the pellet (P1), which was the only fraction that contained detectable levels of the nuclear protein TBP (Figure 5A). At the ultrastructural level, purified synaptosomes contained intact pre- and post-synaptic terminals that were frequently observed in apposition to one another (Figure 5B). The S1 fraction contained some presynaptic structures, but also contained other organelles, including golgi apparatus and endoplasmic reticulum (Figure 5B). The P1 fraction was made up of intact nuclei packed with electron-dense chromatin (Figure 5B). These validation assays demonstrate that purified synaptosomes and the S1 fraction used in subsequent experiments differ in their composition, with significantly greater enrichment of synaptic terminals in the purified preparation.

Primary microglia and peritoneal macrophages from HFD/HFD, HFD/LFD, and LFD/LFD mice were subsequently stimulated with *e.coli* bacteria conjugated to the pH-sensitive fluorophore pHrodo Green. Primary microglia rapidly internalize pHrodo-conjugated *e.coli* based on multiphoton visualization of fixed cells (Figure 5C). The uptake of pHrodo-conjugated *e.coli* was also detectable in plated cells based on fluorometric quantification, which revealed that phagocytosis is more robust in peritoneal macrophages than in primary microglia (Figure 5D; $F_{2,22}=14.70$, $p<0.01$). There was no effect of HFD or diet reversal on *e.coli* internalization in either cell type, suggesting that responses to bacterial pathogens are unaffected by dietary manipulation (Figure 5D).

We next prepared pHrodo-conjugated synaptosomes and S1 fractions to determine whether obesity might influence microglial internalization of synaptic terminals, and whether any potential differences were selective for synapses. Primary microglia from all three groups of mice showed significant uptake of both fractions, based on increased fluorescence intensity relative to unstimulated control wells. However, wells containing HFD/HFD microglia had significantly higher fluorescence intensities after stimulation with synaptosomes, relative to cells from LFD/LFD mice, and relative to cells from HFD/LFD mice (Figure 5D; $F_{2,22}=4.21$, $p<0.05$). There were no differences in the uptake of pHrodo-labeled S1 fractions, suggesting that there is some degree of selectivity in the effects of obesity on microglial phagocytosis (Figure 5D).

4. Discussion

These studies demonstrate that obesity reversibly increases synaptic internalization by microglia. Normal weight mice exhibit minimal overlap between microglia and synaptic markers, but microglial processes were frequently observed in close apposition to clusters of synaptic puncta. Partial attenuation of obesity with diet reversal completely normalized hippocampal function and reinstated spatial relationships between microglia and hippocampal synapses. Dietary obesity increased microglial internalization of purified synaptosomes, but did not alter the uptake of mixed intracellular structures or e.coli bacteria. Take together, these results demonstrate that obesity disturbs microglia/neuron interactions, and implicate synaptic stripping as a potential mechanism for hippocampal dysfunction.

Microglial internalization of synaptic contacts contributes to developmental pruning and regulates activity-dependent synaptic plasticity in the adult brain (Paolicelli et al, 2011; Schafer et al, 2012). We recently demonstrated that obesity promotes the expression of classical activation markers in hippocampal microglia from mice with genetic obesity due to leptin receptor mutation (db/db mice; Erion et al, 2014). However, 'activation' is not always accompanied by increases in phagocytosis (Siskova et al., 2009), and criteria used to define microglial 'activation' varies considerably across studies. Classical activation can be defined using changes in cell-surface antigen expression and reductions in anatomical complexity (Prinz and Priller, 2014), but microglia continually transition between an activated and quiescent phenotype depending on environmental conditions (Hanisch and Kettenmann, 2007). The current study used structural criteria for analysis of MHCII in IBA1+ cells with high or low anatomical complexity. This approach revealed that dietary obesity promotes MHCII expression in morphologically simple microglia, and that diet reversal eliminates both cellular and anatomical activation of IBA1+ cells. Because these static measurements do not capture ongoing structural plasticity, future studies will be required to determine whether and how obesity influences chemoattraction and microglial outgrowth.

Diet reversal reduced body weight, but overall adiposity remained higher than lean controls. Although increases in adiposity were only partially attenuated, deficits in hippocampal plasticity and perturbation of microglia/neuron relationships were completely normalized to within the range of LFD animals. This pattern implies that relationships between adiposity and neuroinflammation in dietary obesity are not simply a linear function of total adiposity or adiposity in the visceral compartment, as observed in genetic obesity (Erion et al., 2014). While visceral adipose tissue is uniformly made up of white adipocytes, subcutaneous adipose tissue contains both white adipocytes and 'beige' adipocytes, which promote energy expenditure in a manner analogous to brown adipose tissue (Spiegelman and Rosen, 2014). Although visceral fat is the primary source of peripheral inflammation in obesity, genetic ablation of beige adipocytes increases inflammation in subcutaneous fat to levels typically observed in the visceral compartment (Cohen et al., 2014). It is tempting to speculate that reversal of microglial activation after a return to LFD might be attributable to reinstatement of the beige adipocyte population, but at present there are no data to support or refute this hypothesis.

The current study used antibodies against ionized calcium binding adapter protein 1 (IBA1) to label microglia, but IBA1 is also expressed by peripheral macrophages (Prinz and Priller, 2014). In a recent report, Buckman et al. (2014) demonstrated infiltration of bone marrow-derived macrophages into the brains of obese mice. This raises the possibility that IBA1-labeled cells in this report may represent a mixed population of infiltrating macrophages and resident microglia. While this possibility cannot presently be excluded, observations from this dataset suggest that this is not the case. Specifically, the total number of IBA1-positive cells determined using unbiased stereology in these experiments was not significantly different between diet conditions. If infiltrating macrophages were present, this would increase total IBA1-positive cell numbers, assuming that there was no concurrent cell death among resident microglia in HFD mice. Because we observed increases in anatomically simple microglia without any significant change in total microglial number, we interpret this result as indirect evidence for minimal macrophage infiltration in the hippocampus. This

interpretation is not inconsistent with the results of Buckman et al. (2014), which reported macrophage infiltration in dissociated forebrains from HFD mice. Regional heterogeneity in macrophage infiltration of different brain regions with obesity is highly likely and will be an interesting question to resolve in future studies.

Converging evidence from animal models and human studies indicates that obesity alters neuronal function in brain regions outside of canonical metabolic circuits. While there is some variability in cognitive outcomes reported in human studies of obesity (Fotuhi et al., 2012), this is likely attributable to the insufficiency of body mass index (BMI) criteria used to define obesity in humans. Weight/height relationships defined by BMI do not reflect body fat distribution, which is a better predictor of cognitive risk (Whitmer et al., 2008). In longitudinal and twin studies, visceral adiposity predicts risk of cognitive decline, but preferential deposition of subcutaneous fat is not associated with age-related cognitive impairment and dementia (Whitmer et al., 2008; Xu et al., 2011). The same pattern is detected in human studies of obesity-induced inflammation, where visceral adiposity increases levels of circulating pro-inflammatory cytokines, but subcutaneous adiposity does not increase systemic markers of inflammation (Chawla et al., 2011; Kanneganti and Dixit, 2012). These findings in humans support the concept of depot-specific effects of adipose tissue on peripheral inflammation and cognitive risk, and data from animal models underscores the complexity of this relationship by identifying distinct consequences of white, beige, and brown adipose tissue for metabolism and potentially, for cognition (Cohen et al., 2014; Rosen and Spiegelman, 2014). The assumption of a linear inverse relationship between body weight and cognition is oversimplified and contributes to pre-existing biases against overweight individuals, and caution against over-interpretation is warranted in clinical and animal model studies. The observations observed in this report indicate that microglial internalization of synapses occurs in a reversible manner with dietary obesity, and further investigation into this process may lead to strategies for preventing age-related cognitive impairment in at-risk populations.

Supplementary Material

Refer to Web version on PubMed Central for supplementary material.

Acknowledgments

These studies were supported by a grant to A.M.S. from the National Institute on Diabetes, Digestive and Kidney Disorders (K01DK100616).

References

Asztely F, Kokaia M, Olofsdotter K, Ortegren U, Lindvall O. Afferent-specific modulation of short-term synaptic plasticity by neurotrophins in dentate gyrus. Eur J Neurosci. 2000; 12:662–669. [PubMed: 10712646]

Bolte S, Cordelieres FP. A guided tour into subcellular colocalization analysis in light microscopy. J Microsc. 2006; 224:213–32. [PubMed: 17210054]

Buckman LB, Hasty AH, Flaherty DK, Buckman CT, Thompson MM, Matlock BK, Weller K, Ellacott KL. Obesity induced by a high-fat diet is associated with increased immune cell entry into the central nervous system. Brain Behav Immun. 2014; 35:33–42. [PubMed: 23831150]

Chawla A, Nguyen KD, Goh YP. Macrophage-mediated inflammation in metabolic disease. Nat Rev Immunol. 2011; 11:738–49. [PubMed: 21984069]

Cohen P, Levy JD, Zhang Y, Frontini A, Kolodin DP, Svensson KJ, Lo JC, Zeng X, Ye L, Khandekar MJ, Wu J, Gunawardana SC, Banks AS, Camporez JP, Jurczak MJ, Kajimura S, Piston DW, Mathis D, Cinti S, Shulman GI, Seale P, Spiegelman BM. Ablation of PRDM16 and beige adipose causes metabolic dysfunction and a subcutaneous to visceral fat switch. Cell. 2014; 156:304–316. [PubMed: 24439384]

Costes SV, Daelemans D, Cho EH, Dobbin Z, Pavlakis G, Lockett S. Automatic and quantitative measurement of protein-protein colocalization in live cells. Biophys J. 2004; 86:3993–4003. [PubMed: 15189895]

Dey A, Hao S, Erion JR, Wosiski-Kuhn M, Stranahan AM. Glucocorticoid sensitization of microglia in a genetic mouse model of obesity and diabetes. J Neuroimmunol. 2014; 269:20–27. [PubMed: 24534266]

Dunkley PR, Jarvie PE, Robinson PJ. A rapid Percoll gradient procedure for preparation of synaptosomes. Nat Protoc. 2008; 3:1718–1728. [PubMed: 18927557]

Erion JR, Wosiski-Kuhn M, Dey A, Hao S, Davis CL, Pollock NK, Stranahan AM. Obesity elicits interleukin 1-mediated deficits in hippocampal synaptic plasticity. J Neurosci. 2014; 34:2618–2631. [PubMed: 24523551]

Fotuhi M, Do D, Jack C. Modifiable factors that alter the size of the hippocampus with ageing. Nat Rev Neurol. 2012; 8:189–202. [PubMed: 22410582]

Giovanoli S, Engler H, Engler A, Richetto J, Voget M, Willi R, Winter C, Riva M, Mortensen PB, Feldon J, Schedlowski M, Meyer U. Stress in puberty unmasks latent neuropathological consequences of prenatal immune activation in mice. Science. 2013; 339:1095–1099. [PubMed: 23449593]

Hanisch UK, Kettenmann H. Microglia: active sensor and versatile effector cells in the normal and pathologic brain. Nat Neurosci. 2007; 10:1387–1394. [PubMed: 17965659]

Kanneganti TD, Dixit VD. Immunological complications of obesity. Nat Immunol. 2012; 13:707–12. [PubMed: 22814340]

Kettenmann H, Kirchhoff F, Verkhratsky A. Microglia: new roles for the synaptic stripper. Neuron. 2013; 77:10–18. [PubMed: 23312512]

McNay EC, Ong CT, McCrimmon RJ, Cresswell J, Bogan JS, Sherwin RS. Hippocampal memory processes are modulated by insulin and high-fat-induced insulin resistance. Neurobiol Learn Mem. 2010; 93:546–553. [PubMed: 20176121]

Meffert MK, Premack BA, Schulman H. Nitric oxide stimulates calcium-independent synaptic vesicle release. Neuron. 1994; 12:1235–1244. [PubMed: 7912090]

Molteni R, Barnard RJ, Ying Z, Roberts CK, Gómez-Pinilla F. A high-fat, refined sugar diet reduces hippocampal brain-derived neurotrophic factor, neuronal plasticity, and learning. Neuroscience. 2002; 112:803–814. [PubMed: 12088740]

Paolicelli RC, Bolasco G, Pagani F, Maggi L, Scianni M, Panzanelli P, Giustetto M, Ferreira TA, Guiducci E, Dumas L, Ragozzino D, Gross CT. Synaptic pruning by microglia is necessary for normal brain development. Science. 2011; 333:1456–1458. [PubMed: 21778362]

Parkhurst CN, Yang G, Ninan I, Savas JN, Yates JR 3rd, Lafaille JJ, Hempstead BL, Littman DR, Gan WB. Microglia promote learning-dependent synapse formation through brain-derived neurotrophic factor. Cell. 2013; 155:1596–1609. [PubMed: 24360280]

Prinz M, Priller J. Microglia and brain macrophages in the molecular age: from origin to neuropsychiatric disease. Nat Rev Neurosci. 2014; 15:300–312. [PubMed: 24713688]

Rosen ED, Spiegelman BM. What we talk about when we talk about fat. Cell. 2014; 156:20–44. [PubMed: 24439368]

Schafer DP, Lehrman EK, Kautzman AG, Koyama R, Mardinly AR, Yamasaki R, Ransohoff RM, Greenberg ME, Barres BA, Stevens B. Microglia sculpt postnatal neural circuits in an activity and complement-dependent manner. Neuron. 2012; 74:691–705. [PubMed: 22632727]

Sisková Z, Page A, O'Connor V, Perry VH. Degenerating synaptic boutons in prion disease: microglia activation without synaptic stripping. Am J Pathol. 2009; 175:1610–1621. [PubMed: 19779137]

Sobesky JL, Barrientos RM, De May HS, Thompson BM, Weber MD, Watkins LR, Maier SF. High-fat diet consumption disrupts memory and primes elevations in hippocampal IL-1β, an effect that can be prevented with dietary reversal or IL-1 receptor antagonism. Brain Behav Immun. 2014; 42:22–32. [PubMed: 24998196]

Stevens B, Allen NJ, Vazquez LE, Howell GR, Christopherson KS, Nouri N, Micheva KD, Mehalow AK, Huberman AD, Stafford B, Sher A, Litke AM, Lambris JD, Smith SJ, John SW, Barres BA. The classical complement cascade mediates CNS synapse elimination. Cell. 2007; 131:1164–1178. [PubMed: 18083105]

Stranahan AM. Models and mechanisms for hippocampal dysfunction in obesity and diabetes. Neuroscience. 2015 pii:S0306–4522(15)00386–3.

Stranahan AM, Norman ED, Lee K, Cutler RG, Telljohann RS, Egan JM, Mattson MP. Diet-induced insulin resistance impairs hippocampal synaptic plasticity and cognition in middle-aged rats. Hippocampus. 2008; 18:1085–1088. [PubMed: 18651634]

Whitmer RA, Gustafson DR, Barrett-Connor E, Haan MN, Gunderson EP, Yaffe K. Central obesity and increased risk of dementia more than three decades later. Neurology. 2008; 71:1057–1064. [PubMed: 18367704]

Wosiski-Kuhn M, Erion JR, Gomez-Sanchez EP, Gomez-Sanchez CE, Stranahan AM. Glucocorticoid receptor activation impairs hippocampal plasticity by suppressing BDNF expression in obese mice. Psychoneuroendocrinology. 2014; 42:165–77. [PubMed: 24636513]

Wosiski-Kuhn M, Stranahan AM. Transient increases in dendritic spine density contribute to dentate gyrus long-term potentiation. Synapse. 2012; 66:661–664. [PubMed: 22314918]

Xu WL, Atti AR, Gatz M, Pedersen NL, Johansson B, Fratiglioni L. Midlife overweight and obesity increase late-life dementia risk: a population-based twin study. Neurology. 2011; 76:1568–1574. [PubMed: 21536637]

Research Highlights

- Dietary obesity impairs hippocampus-dependent memory and long-term potentiation
- High-fat diet promotes anatomical simplification and induction of activation markers in hippocampal microglia
- Diet reversal reinstates microglial quiescence and normalizes hippocampal function
- Primary microglia from mice with dietary obesity exhibit selective increases in synaptic phagocytosis

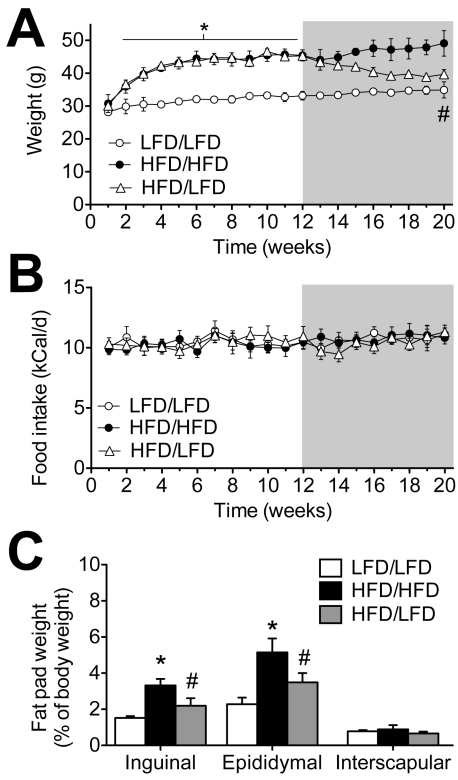

Figure 1. Changes in body weight, food intake, and adiposity after switching from high-fat to low-fat diet

(A), Male C57Bl6J mice maintained on a 60% fat diet (HFD) gain weight rapidly, but when switched to a low-fat diet (HFD/LFD), their weight gradually declines until it is comparable with mice never been exposed to HFD feeding (LFD). Shaded area represents the duration of diet reversal (weeks 12–20). (B), Mice on HFD chow reduce the amount of food eaten and are isocaloric with LFD mice. (C), Overconsumption of calories from fat increases the proportional weight of adipose tissue in the subcutaneous and visceral depots. Adipose tissue hypertrophy is attenuated but not reversed in HFD/LFD mice. For all graphs, error bars represent the s.e.m., and asterisks (*) denote significant differences between HFD/HFD and LFD/LFD mice. Pound signs (#) indicate differences between HFD/HFD and HFD/LFD mice. Data were analyzed using one-way repeated measures ANOVA (A–B) or one-way ANOVA (C) with significance at $p<0.05$ and post hoc Bonferroni-corrected t-tests.

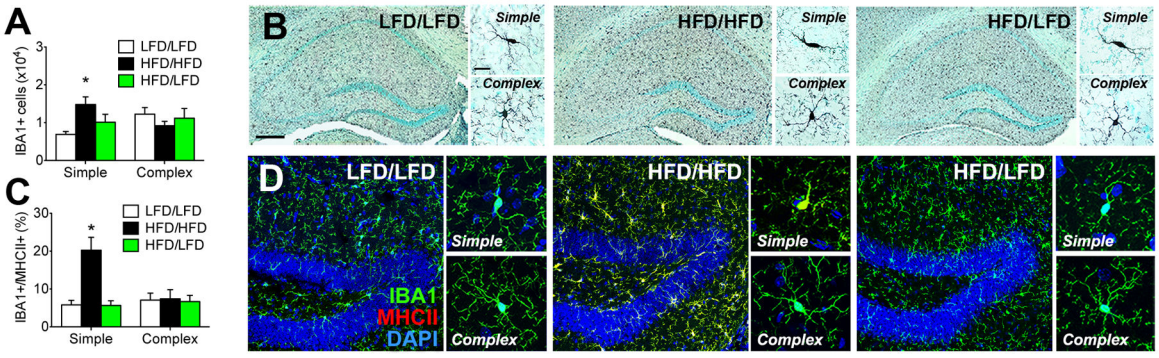

Figure 2. High-fat diet consumption reversibly activates hippocampal microglia

(A), Stereological quantification of microglia in the hippocampal dentate gyrus reveals that mice consuming high-fat diet throughout the experiment (HFD/HFD) have significantly more microglia with 1–2 primary processes ('Simple'). By contrast, mice exposed to 3 months of HFD, then switched to low-fat diet (LFD) chow for 2 months (HFD/LFD) have fewer simple microglia than HFD/HFD mice. There was no effect of HFD or diet reversal on microglia with 3 or more primary processes ('Complex'). (B), Micrographs depict peroxidase immunolabeling for the microglial marker ionized calcium binding adapter protein 1 (IBA1) on hippocampal sections from mice in the indicated conditions. Higher magnification panels show Simple and Complex microglia from mice in each condition. For low magnification images, scalebar=100μm. For high magnification panels, scalebar=10μm. (C), Expression of the classical activation marker major histocompatibility complex II (MHCII) is sparse in IBA1+ cells from LFD/LFD and HFD/LFD mice, regardless of their morphology, but HFD/HFD mice exhibit robust induction of MHCII in anatomically simple microglia. (D), Confocal micrographs of IBA1/MHCII fluorescence, with DAPI nuclear counterstain. Scalebar=5μm. For all graphs, error bars represent the s.e.m. and asterisks (*) denote statistical significance at $p<0.05$ following one-way ANOVA with post hoc Bonferroni-correct t-tests.

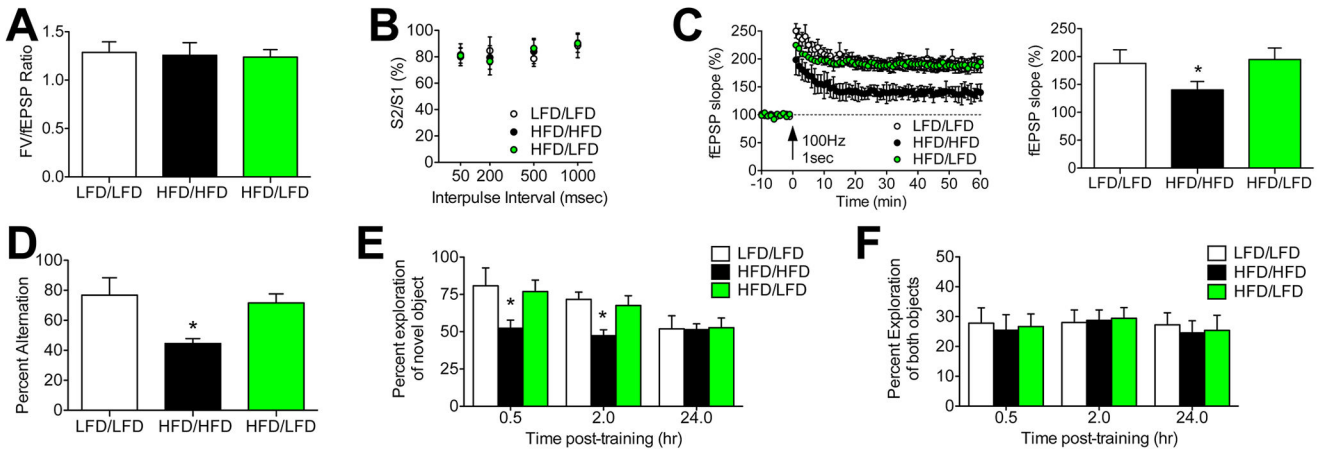

Figure 3. Diet reversal rescues synaptic plasticity and cognition

(A), Dietary obesity and diet reversal do not influence the input/output ratio, derived from the amplitude of the presynaptic fiber volley (FV) and the slope of the dendritic field excitatory postsynaptic potential (fEPSP). (B), Presynaptic paired-pulse plasticity is unaffected by HFD or diet reversal. (C), Dietary obesity impairs dentate gyrus long-term potentiation (LTP), but HFD/LFD mice exhibit LTP that is identical to LFD/LFD mice. Bar graph (right) depicts percent change in fEPSP slope during minutes 50–60 of recording. (D), HFD impairs spatial recognition memory, based on reduced alternation in the Y-maze. HFD/LFD mice alternate at rates that are similar to LFD/LFD mice, consistent with reinstatement of spatial recognition memory with diet reversal. (E), Dietary obesity impairs object recognition, based on the lack of preference for a novel object over a familiar one in HFD/HFD mice. Preference for the novel object is normalized in HFD/LFD mice, which perform on par with LFD/LFD mice at 0.5 and 2.0hr after initial object exposure. (F), The total amount of exploration (novel + familiar) as a proportion of test session duration was unaffected by HFD or diet reversal. For all graphs, error bars represent the sem and asterisks (*) denote statistical significance at $p<0.05$ following one-way ANOVA with post hoc Bonferroni-corrected t-tests.

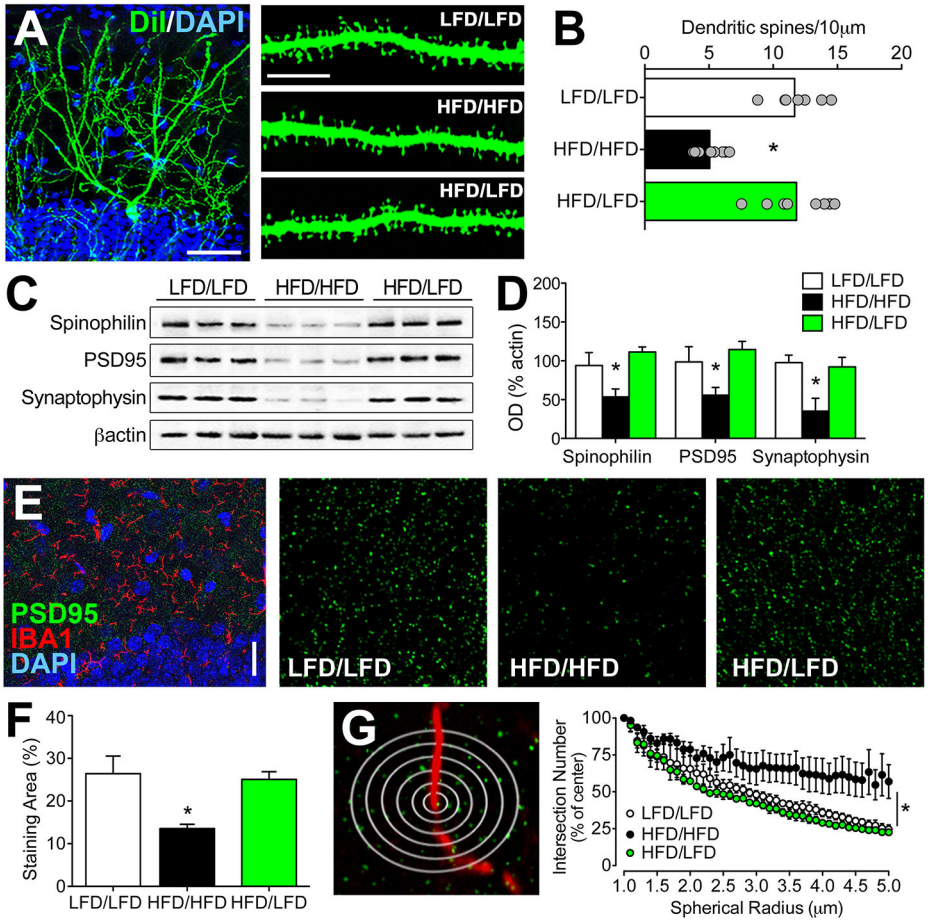

Figure 4. Perturbation of spatial relationships between hippocampal synapses and microglia coincides with obesity-induced reductions in dendritic spines and synaptic marker expression

(A), Low-magnification confocal micrograph shows a dentate granule cell labeled with DiI (green) and counterstained with DAPI (blue). Scalebar=50μm. High magnification panels (right) depict dendritic segments from mice in each condition. Scalebar=10μm. (B), High-fat diet (HFD/HFD) reduces dendritic spine density relative to low-fat diet (LFD/LFD) mice, but deficits are not present among dentate granule neurons from mice exposed to diet reversal (HFD/LFD). Bar graphs depict the group mean and scatterplots show data from individual animals (average of 5–7 cells per animal). (C), Western blot membranes depict representative band intensities for the postsynaptic markers spinophilin and PSD95, and the presynaptic marker synaptophysin. (D), Dietary obesity reversibly impairs hippocampal synaptic protein expression. (E), Low-magnification micrograph shows immunofluorescence labeling for the microglial marker IBA1 and the synaptic marker PSD95. High-magnification single-channel images (right) depict punctate staining for PSD95 in the dentate molecular layer. (F), HFD/HFD mice exhibit reduced total area of PSD95 labeling, but HFD/LFD mice exhibit similar staining area relative to LFD/LFD mice. (G), Schematic shows flattened depiction of multichannel Sholl analysis. PSD95+ intersections were quantified in concentric spheres (0.1μm radius) around IBA1-labeled processes and were expressed relative to the number of intersections in the initial spherical shell to eliminate the

confound of reduced overall PSD95 labeling in HFD/HFD mice. Graph (right) demonstrates non-random organization of PSD95 puncta around IBA1+ processes, based on progressively decreasing PSD95+ puncta at greater distances from microglial processes in LFD/LFD mice. While this relationship is detectable in HFD/HFD mice, the slope is significantly reduced based on comparative nonlinear regression analysis. Diet reversal normalizes spatial relationships between microglial processes and synaptic puncta, indicated by similar statistical methods of comparison described above. For all graphs, error bars represent the sem. For graphs in (A–F), asterisks (*) denote statistical significance at $p<0.05$ following one-way ANOVA with post hoc Bonferroni-corrected t-tests. For graph in (G), asterisk indicates statistical significance determined by generating per-animal slopes for the relationship between the normalized number of PSD95+ intersections and distance from IBA1+ processes using nonlinear regression, and comparing the slopes across animals in different conditions using one-way ANOVA as described above.

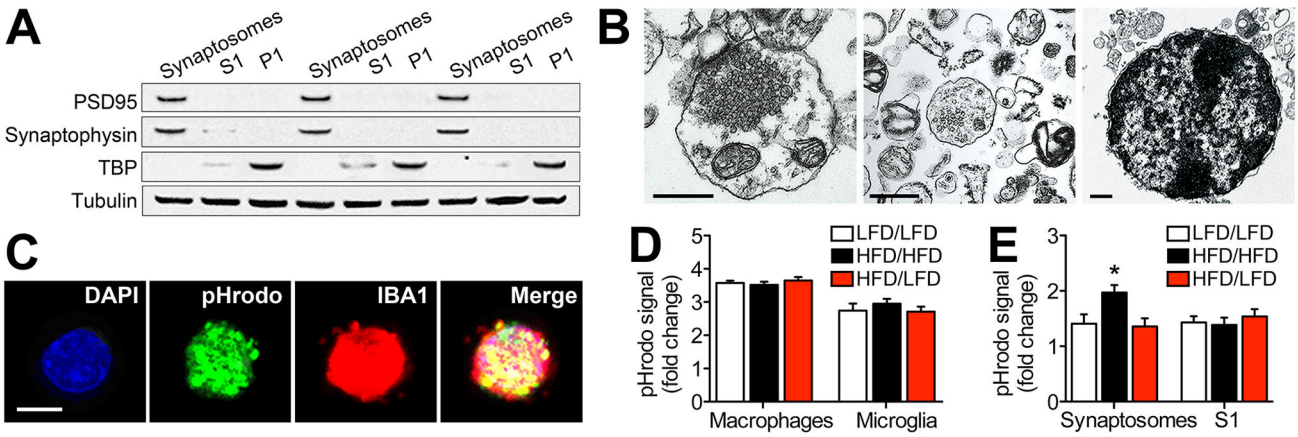

Figure 5. Obesity reversibly increases synaptic internalization by microglia

(A), Purified synaptosomes are highly enriched with PSD95 and synaptophysin than mixed cellular organelles in the S1 fraction. Nuclear protein TBP was only detected in the P1 fraction. (B), Visualization of purified synaptosomes (left), S1 fraction (middle), and P1 fraction (right) by electron microscopy. Scalebar = 500nm. (C), Primary microglia incubated with e.coli conjugated to the pH-sensitive fluorophore pHrodo Green (pHrodo) internalize e.coli and express the microglial marker IBA1. (D), Fluorometric quantification of pHrodo-conjugated e.coli in peritoneal macrophages and primary microglia revealed no significant effects of obesity or diet reversal. (E), Internalization of pHrodo-conjugated synaptosomes is significantly greater in primary microglia from mice on a high-fat diet (HFD/HFD), relative to cells from low-fat diet mice. Synaptosome internalization in HFD mice exposed to diet reversal (HFD/LFD) is indistinguishable from LFD/LFD mice. Internalization of pHrodo-conjugated mixed organelles (S1 fraction) was similar across all conditions, indicative of selective increases in synaptic phagocytosis in dietary obesity. For all graphs, error bars represent the sem and asterisks (*) denote statistical significance at $p<0.05$ following one-way ANOVA with post hoc Bonferroni-corrected t-tests.